Examining Efficacy of "TAT-less" Delivery of a Peptide against the L-Type Calcium Channel in Cardiac Ischemia–Reperfusion Injury

Tristan D. Clemons,[†,⊥] Helena M. Viola,[‡,⊥] Michael J. House,[§] K. Swaminathan Iyer,[†] and Livia C. Hool[‡,*]

[†]School of Chemistry and Biochemistry, The University of Western Australia, Crawley, WA, 6009, Australia, [‡]School of Anatomy, Physiology and Human Biology, The University of Western Australia, Crawley, WA, 6009, Australia, and [§]School of Physics, The University of Western Australia, Crawley, WA, 6009, Australia. [⊥]T.D.C. and H.M.V. contributed equally to this work.

ABSTRACT Increased calcium influx through the L-type Ca^{2+} channel or overexpression of the alpha subunit of the channel induces cardiac hypertrophy. Cardiac hypertrophy results from increased oxidative stress and alterations in cell calcium levels following ischemia–reperfusion injury and is an independent risk factor for increased morbidity and mortality. We find that decreasing the movement of the auxiliary beta subunit with a peptide derived against the alpha-interacting domain (AID) of the channel attenuates ischemia–reperfusion injury. We compared the efficacy of delivering the AID peptide using a trans-activator of transcription (TAT) sequence with that of the peptide complexed to multifunctional polymeric nanoparticles. The AID-tethered nanoparticles perfused through the myocardium more diffusely and associated with cardiac myocytes more rapidly than the TAT-labeled peptide but had similar effects on intracellular calcium levels. The AID-complexed nanoparticles resulted in a similar reduction in release of creatine kinase and lactate dehydrogenase after ischemia–reperfusion to the TAT-labeled peptide. Since nanoparticle delivery also holds the potential for dual drug delivery, we conclude that AID-complexed nanoparticles may provide an effective platform for peptide delivery in cardiac ischemia–reperfusion injuries.

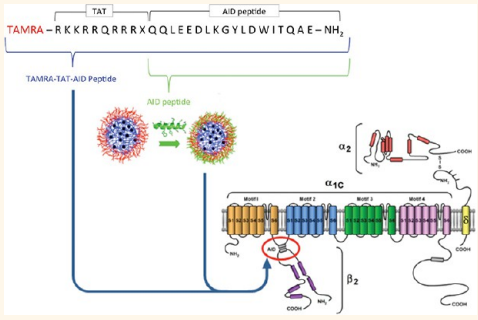

KEYWORDS: peptide delivery · nanoparticle · ischemia–reperfusion

Myocardial ischemia–reperfusion injury is the primary contributor to the morbidity and mortality associated with coronary artery disease. Ischemia–reperfusion has been reported to result in an increase in reactive oxygen species (ROS) and intracellular calcium, which contribute to the development of cardiac hypertrophy and cardiac failure.[1−4] Previous work has shown that minimizing myocardial damage and oxidative stress during reperfusion is directly related to a decrease in morbidity and mortality.[5−8] During ischemia–reperfusion, multiple perturbations in cell ion homeostasis lead to alterations in mitochondrial function that further contribute to oxidative stress and compromised energetics. Damage to the mitochondrial electron transport chain results in increased mitochondrial generation of ROS, which leads to opening of the mitochondrial permeability transition pore, rupture of the plasma membrane, and subsequent cell death.[3,9]

It is now well established that intracellular Ca^{2+} is an integral component of cell function as an important signaling molecule and also as a regulator of adenosine-5′-triphosphate (ATP) production by mitochondria.[10,11] However, significant increases in intracellular Ca^{2+} that occur during reperfusion are deleterious to cell function, as they can lead to further production of ROS by the mitochondria and activation of apoptotic and necrotic pathways.[3,9] Thus, minimizing Ca^{2+} influx during reperfusion is critical to preventing damage associated with reperfusion injury. In addition, therapeutic intervention with antioxidants to attenuate the increase in ROS during injury has had varied success in limiting cardiac damage and hypertrophy, with some studies demonstrating a

* Address correspondence to livia.hool@uwa.edu.au.

Received for review November 9, 2012 and accepted February 22, 2013.

Published online February 22, 2013
10.1021/nn305211f

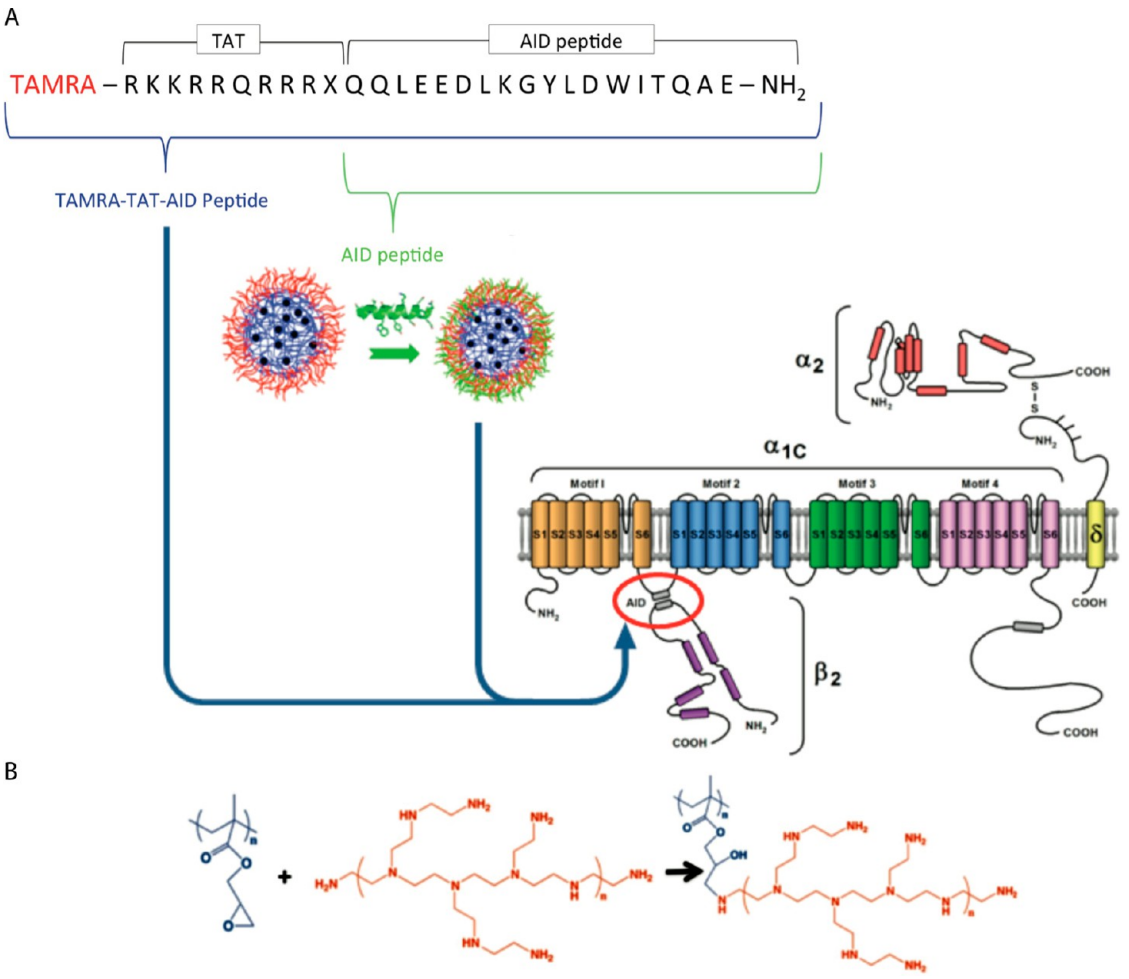

Figure 1. Schematic representation of AID peptide loaded nanoparticles (AID-NP) and TAT-bound AID (AID-TAT). (A) Sequence of TAMRA-labeled AID peptide including TAT sequence. Site of attachment to alpha interacting domain (AID) of the L-type Ca^{2+} channel is shown. (B) Epoxide attachment of PEI polymer chains to the PGMA nanoparticle surface.

reduction in infarct size with antioxidant treatment,[12−14] while others showing no significant difference at all.[15−17]

The L-type Ca^{2+} channel is the main route for calcium influx into cardiac myocytes. Since activation of the L-type Ca^{2+} channel during oxidative stress can lead to further oxidative stress and induction of myocyte hypertrophy,[1,2] modifying the function of the L-type Ca^{2+} channel during reperfusion may hold the key to protection against myocardial damage. The L-type Ca^{2+} channel is a heterotetramer comprising three subunits, an α_{1C} subunit, a β_2 subunit, and an $\alpha_2\delta$ subunit (Figure 1A). The α_{1C} subunit is required for ion conductance and is sufficient in the absence of accessory subunits. The β_2 subunit binds to the α_{1C} subunit at the alpha interacting domain (AID) and assists with the trafficking of the α_{1C} subunit to the cellular membrane.[18,19] The β_2 subunit also regulates the inactivation of the α_{1C} subunit.[18,19] Previous studies have demonstrated an important role of AID in modulating this response. Application of a synthetic peptide corresponding to the sequence of AID significantly inhibits the interaction between the α_{1C} and β subunits of the channel and alters inactivation kinetics of the channel.[20]

We propose a unique approach to regulate channel function during reperfusion by targeting the AID region of the α_{1C} subunit rather than directly altering calcium influx through the S5−S6 pore region of the α_{1C} subunit of the channel. The rationale for this is that we propose to manipulate channel function at a concentration of the peptide that does not alter calcium influx and thereby prevents negative inotropic effects. Therefore, delivery of a peptide that binds to the AID region may provide an effective therapeutic intervention by preventing the movement of the β_2 subunit during activation of the channel.

A current and widely used strategy for the effective delivery of therapeutic peptides, proteins, and nucleic acids is *via* conjugation with cell-penetrating peptides (CPPs), also referred to as protein transduction domains (PTDs). The TAT peptide sequence is one of the most widely researched CPPs.[21] TAT is an 11 residue long peptide taken from the HIV-1 TAT protein that activates

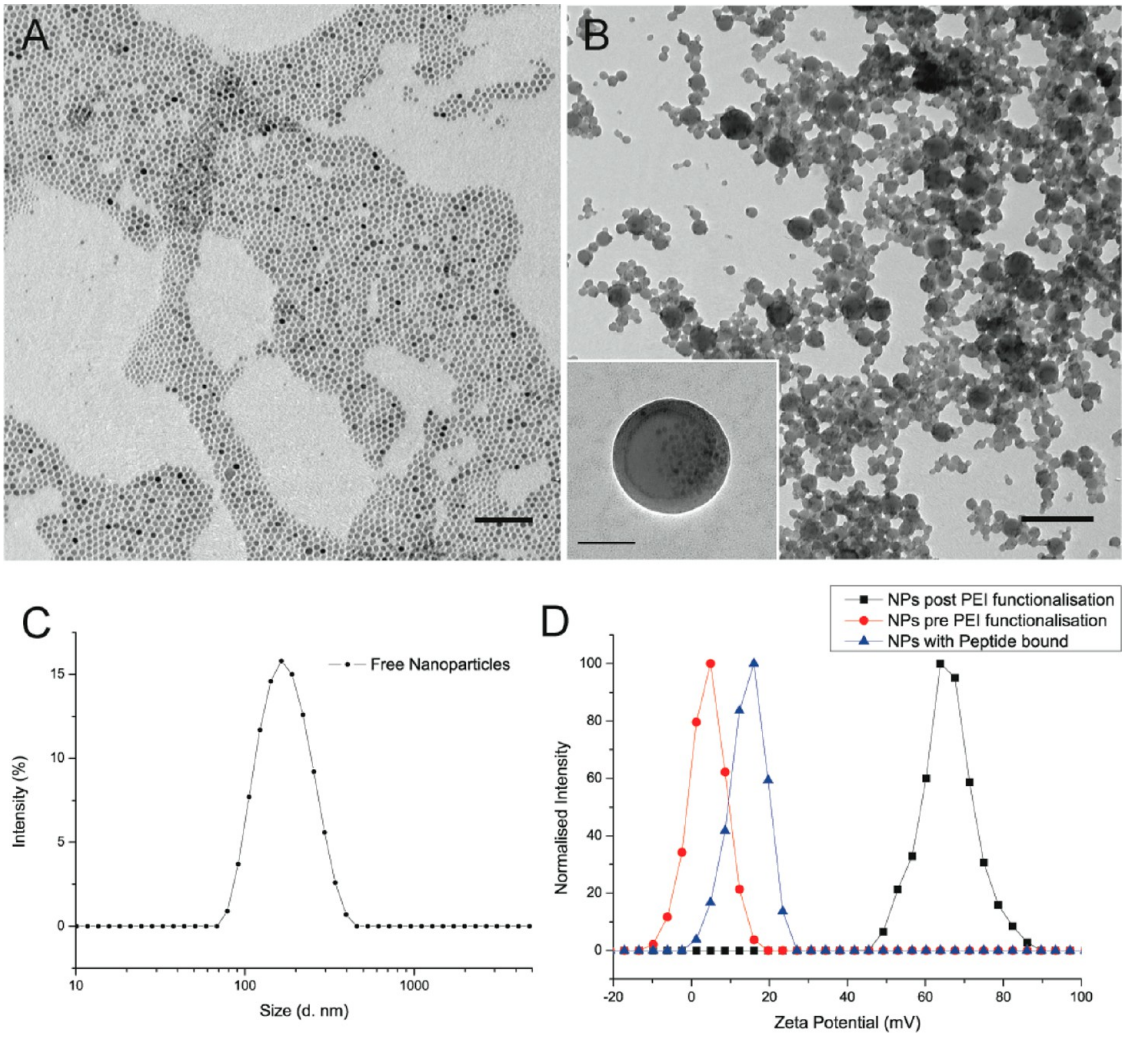

Figure 2. Characteristics of nanoparticles. (A) TEM image of magnetite nanoparticles, scale 100 nm. (B) TEM image of polymeric nanoparticles containing encapsulated magnetite without AID peptide loading, scale 500 nm with high magnification inset, inset scale 50 nm. (C) Particle size distribution by dynamic light scattering. (D) Zeta potential of the nanoparticles before PEI functionalization (red), with PEI functionalization (black), and with AID peptide conjugated to the PEI-functionalized nanoparticle surface (blue).

transcription of the viral genome and is a responsible factor for the virus' transfection.[22] TAT is rich in arginine and lysine residues, making it a highly charged, basic, and hydrophilic peptide suitable for attachment to the anionic cell membrane and subsequent cargo delivery.[21−24] TAT conjugation has been used for the delivery of a range of cargoes including peptides, proteins,[25] and nanoparticles.[26,27] However, the safety of the use of TAT as therapy is still uncertain, as questions remain regarding the toxicity and immunogenicity of TAT peptides. It has been speculated that TAT, especially through repeated dosing, may produce a significant immunogenic response, thus limiting its clinical applications;[22] however other studies have provided data presenting low toxicity of the TAT peptide when used for delivery.[28,29] In this report, we compare TAT-mediated delivery and nanoparticle -mediated delivery of the AID peptide (Figure 1). The two modes of delivery are compared in an *ex vivo* model of cardiac ischemia−reperfusion injury.

RESULTS AND DISCUSSION

The nanoparticle used in the current study consists of a rhodamine B-polyglycidal methacrylate core (RhB-PGMA) containing encapsulated magnetite (Fe_3O_4) nanoparticles. Polyethyleneimine (PEI) was covalently bound to the RhB-PGMA core to facilitate a cationic surface suitable for electrostatic conjugation with the AID peptide and to facilitate cell membrane interaction. We exploited the epoxide functionality of poly(glycidyl methacrylate) (PGMA) to covalently attach cationic rhodamine B and PEI to the nanoparticle surface. This results in strong AID peptide complexation with the nanoparticle surface. Previous studies demonstrate that this covalent attachment of PEI to multiple epoxy groups of the PGMA core renders the nanoparticle nontoxic in both *in vitro*[30] and *in vivo*[31] settings. Furthermore, the presence of magnetite serves a twofold function. First, it is a potential MRI contrast agent for *in vivo* tracking, as the nanoparticles were

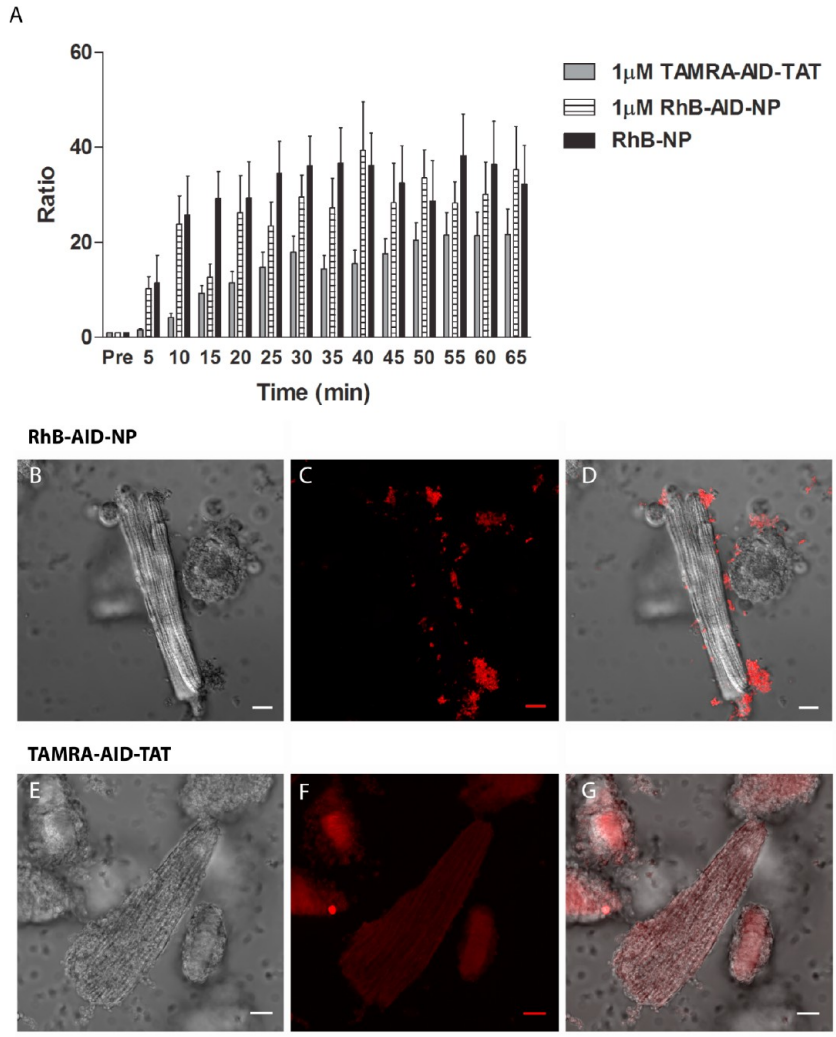

Figure 3. Myocytes take up AID-tethered nanoparticles more rapidly than AID-TAT. (A) Fluorescent uptake of RhB-AID-NP and TAMRA-AID-TAT association with cardiac myocytes over changes in time. Minimum $n = 12$ per time point, per sample. (B–D) Images of a guinea pig cardiac myocyte following 5 h incubation with 1 μM RhB-AID-NP. (B) Confocal DIC. (C) Fluorescent RhB signal. (D) Confocal DIC image overlaid with fluorescent RhB signal. (E–G) Images of a cardiac myocyte following 4.5 h incubation with 1 μM AID-TAT-TAMRA. (E) Confocal DIC. (F) Fluorescent TAMRA signal. (G) Confocal DIC image overlaid with fluorescent TAMRA signal. All scale bars 10 μm.

superparamagnetic, as determined by SQUID magnetometry with no magnetic hysteresis at 300 K (with specific saturation magnetization of 6 emu g^{-1}) and the transverse relaxivity r_2 of the nanoparticle determined, based on the iron content inside the polymer, to be 340 s^{-1} mM^{-1} Fe.[30] Second, and most importantly, the presence of magnetite provides a means to separate, wash, and concentrate the nanoparticles using a magnetic fractionation column suitable for peptide conjugation. The nanoparticles used in the current study had an average size of 160 nm (95% confidence interval 85–342 nm) and a positive surface charge of 65 mV (Figure 2). The AID peptide was complexed to the nanoparticles through the favorable electrostatic interactions between the negative residues on the peptide and the cationic PEI grafted to the nanoparticle surface. Peptide loading on the nanoparticles was determined to be 0.072 nM AID peptide/μg nanoparticles (0.16 w/w %) (Figure S1 Supporting Information). The loading of peptide on the nanoparticles without PEI surface functionalization was determined to be 0.024 nM AID peptide/μg nanoparticles (0.05 w/w %), hence providing evidence for the PEI inclusion, resulting in a 3-fold increase in peptide loading with the nanoparticles.

The nanoparticle–AID peptide complexes were adjusted for optimal peptide concentration with a stock solution of 100 μM peptide in sterile milli-Q water, which was subsequently diluted to either 1 or 10 μM peptide for all experiments with comparison to the same concentration of AID-TAT in the *ex vivo* ischemia–reperfusion injury model.

Both delivery systems were initially investigated for their rate of association with cardiac myocytes. Primary isolates of guinea pig cardiac myocytes were exposed

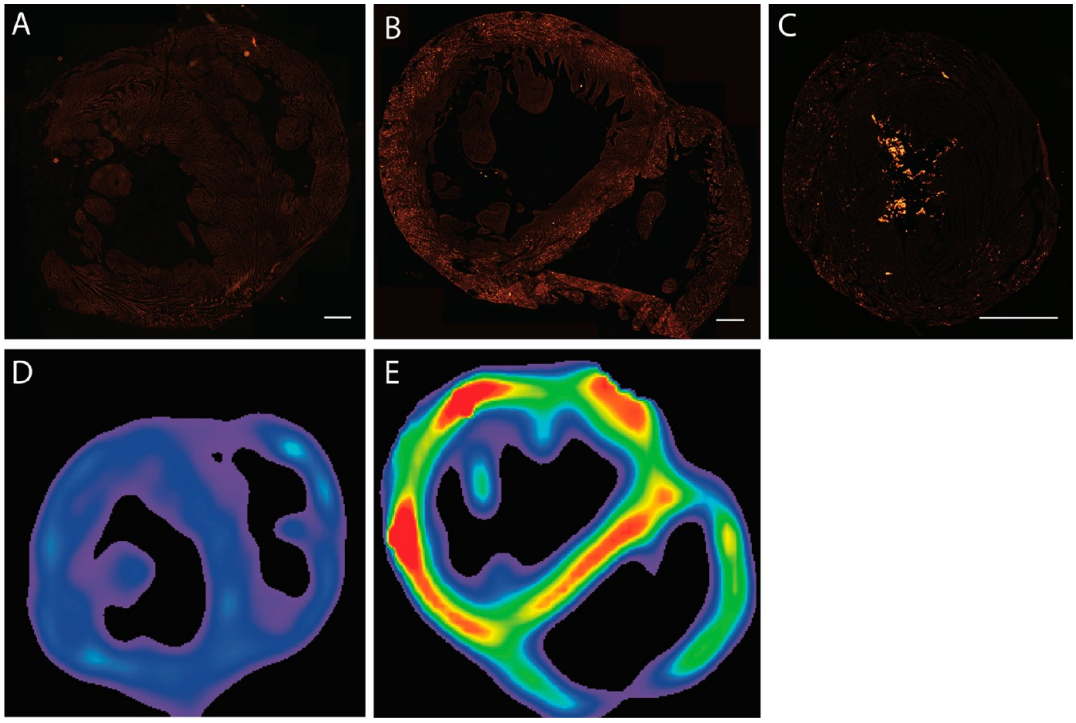

Figure 4. Assessment of biodistribution of AID in hearts perfused with either AID-NP or TAMRA-AID-TAT. (A) Fluorescent microscopy of a heart perfused with KHB only (no therapeutic delivery) for 30 min. (B) Fluorescent microscopy of a heart perfused with KHB supplemented with 1 μM AID-NP for 30 min. (C) Fluorescent microscopy of a heart perfused with KHB supplemented with 1 μM AID-TAT-TAMRA for 30 min. (D) R_2 MRI map of heart perfused only with KHB (*i.e.*, heart shown in panel A) for 30 min. (E) R_2 MRI map of heart perfused with KHB supplemented with 1 μM AID-NP (*i.e.*, heart shown in panel B) for 30 min. Note the brighter, higher R_2 values, indicating accumulation of nanoparticles.

to 1 μM AID-TAT peptide labeled with carboxytetramethylrhodamine (TAMRA). Uptake of the TAMRA-labeled peptide (TAMRA-AID-TAT) was measured as an increase in fluorescence over time relative to background levels. Maximal association of TAMRA-AID-TAT with myocytes occurred at 35 min (n = 14, Figure 3A). We then compared uptake of the AID-TAT peptide with that of the AID peptide (minus TAT) complexed to the polymeric nanoparticles, making use of the nanoparticles covalently binding rhodamine B (RhB) for fluorescent tracking. In contrast to the TAT-linked peptide, the AID peptide complexed to nanoparticles (RhB-AID-NP) associated with cells more rapidly, with a maximal fluorescent signal occurring at 15 min (Figure 3A). It is noteworthy that the peptide complexed to the nanoparticles did not significantly affect the association of the nanoparticles with the cells (Figure 3A nanoparticles alone, RhB-NP). Furthermore, zeta potential measurements indicated that the peptide-complexed nanoparticles had a net positive charge of 18 mV in comparison to a 65 mV charge on the cationic PEI decorated nanoparticles (Figure 2D). Confocal imaging of the peptide complexed to nanoparticles (labeled with RhB) and TAMRA-labeled TAT-peptide demonstrated similar cellular association for both modes of delivery after 5 and 4.5 h of incubation, respectively (Figure 3B–G). Additionally, confocal analysis also revealed that the two modes of delivery operated differently in an *in vitro* setting. The TAT-based delivery showed internalization of the peptide following incubation with myocytes; however the nanoparticles were mainly associated with the cell surface (Figure 3D,G and Figure S2 video of confocal Z-stack reconstruction in the Supporting Information). The region of the L-type calcium channel targeted by the AID peptide is found intracellular and close to the cellular membrane; hence association with the lipid bilayer of the cells is proximal to the intended delivery site and is likely to be sufficient for effective delivery of the AID peptide.

We next examined the distribution of the peptide in the myocardium using the two modes of delivery. Perfusion of 1 μM RhB-AID-NP into the coronary arteries of healthy hearts resulted in a dense and wide distribution of nanoparticles throughout the tissue when assessed by magnetic resonance imaging as well as fluorescent microscopy when compared to controls (buffer reperfusion only) (Figure 4A,B). In comparison, perfusion of 1 μM TAMRA-AID-TAT resulted in a more sparse distribution assessed by fluorescence microscopy (Figure 4C). It is anticipated that the wider and more dense distribution in the heart muscle by the nanoparticles is further support of the data presented in Figure 2A, where it is evident the nanoparticles are able to associate more rapidly with myocytes in comparison with the AID-TAT peptide, especially over the longer time frame assessed during the perfusion.

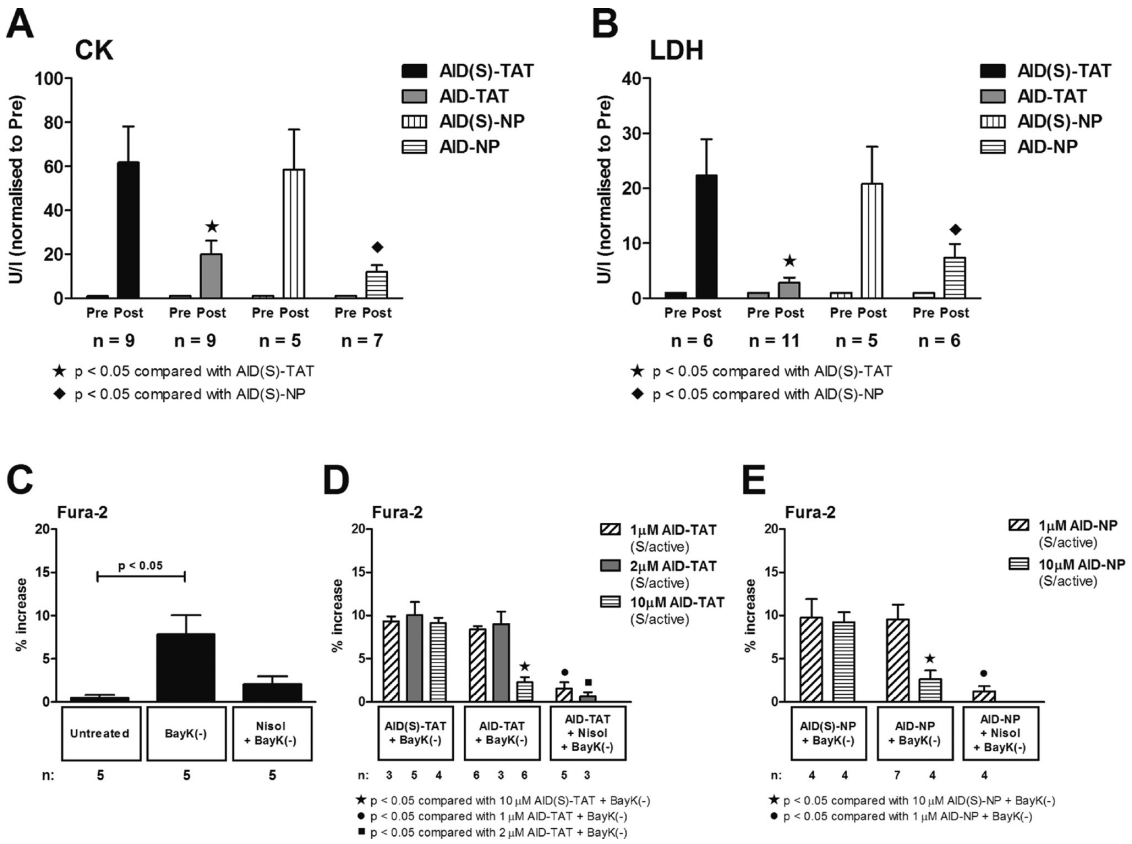

Figure 5. Comparison of effects of AID-TAT and AID-NP on damage assessment *ex vivo* and intracellular calcium *in vitro*. (A) Creatine kinase (CK) and (B) lactate dehydrogenase (LDH) levels were assessed in perfusate taken before (Pre) and after (Post) ischemia−reperfusion in the presence of AID(S)-TAT, AID-TAT, AID(S)-NP, or AID-NP as indicated (see text for detail). (C−E) Fura-2 was used to assess alterations in intracellular calcium in myocytes following addition of the L-type Ca^{2+} channel agonist BayK(−) alone or BayK(−) plus Nisol (C) or in the presence of AID-TAT (D) or AID-NP (E) as indicated. Nisol: nisoldipine (L-type Ca^{2+} channel antagonist).

Finally we assessed the efficacy of the AID peptide in alleviating damage in an *ex vivo* guinea pig cardiac ischemia−reperfusion model making use of both delivery systems. Hearts were isolated from adult guinea pigs and were then perfused retrogradely on a Langendorff apparatus with Ca^{2+}-containing Krebs solution for 30 min, followed by no flow ischemia for 30 min and then reperfusion for 30 min in the presence of 1 μM AID-TAT peptide (AID-TAT), 1 μM scrambled AID-TAT peptide (AID(S)-TAT), AID-complexed nanoparticles (AID-NP), or scrambled AID-complexed nanoparticles (AID(S)-NP). Damage was assessed by comparing the release of creatine kinase (CK) and lactate dehydrogenase (LDH) in the perfusate collected during reperfusion to the levels pre-reperfusion. Application of 1 μM AID-NP was as effective as 1 μM AID-TAT at preventing CK release and similarly at decreasing LDH release, with both delivery systems producing significant improvements when compared to the AID(S)-TAT or AID(S)-NP controls (Figure 5A,B).

Intracellular Ca^{2+} plays an integral role in cardiac function. Calcium influx is critical to cardiac excitation and contraction.[32] Calcium influx is also necessary for release of calcium from intracellular stores and actin/myosin interaction for contraction.[32,33] Intracellular Ca^{2+} levels were assessed as changes in Fura-2 fluorescence after activation of the L-type Ca^{2+} channel with application of the dihydropyridine receptor (DHPR) agonist BayK(−). Consistent with previous reports,[34] BayK(−) alone resulted in an 8% increase in Fura-2 signal, and the L-type Ca^{2+} channel antagonist nisoldipine (Nisol) attenuated the increase in Fura-2 after application of BayK(−) (Figure 5C). Application of 1 μM AID-TAT or 1 μM AID-NP had no effect on the Fura-2 signal after application of BayK(−) (Figure 5D,E). However, application of 2 or 10 μM AID-TAT resulted in a decrease in the BayK(−)-stimulated Fura-2 signal (Figure 5D). Similar results were recorded with AID-NP (Figure 5E). These results suggest that 1 μM AID peptide is an effective concentration to decrease ischemia−reperfusion injury without altering Ca^{2+} influx.

CONCLUSIONS

The delivery of the AID peptide on the polymeric nanoparticle was more rapidly taken up into the myocyte and was more widely distributed in the myocardium than when the peptide was delivered using the HIV-derived TAT sequence (Figures 3 and 4). Although not addressed here, an additional advantage

of the nanoparticle-based system is a platform for intervention using multiple payloads combined within a single delivery platform that is currently unattainable using TAT-mediated delivery. We conclude that AID-TAT and AID-complexed nanoparticles provide effective modes of delivery of the AID peptide in the heart. Both modes of delivery were efficacious in reducing damage associated with ischemia–reperfusion. Therefore this study provides justification for further development of the techniques for tolerance as a therapy in the clinical setting.

METHODS

Nanoparticle Synthesis. *Materials.* Chemicals were purchased from Sigma-Aldrich unless otherwise stated: benzyl ether (99%), ethyl methyl ketone (MEK), iron(III) acetylacetonate (97%), oleic acid (BDH, 92%), oleyl amine (70%), Pluronic F108, polyethylenimine (PEI 50% solution, M_n 1200, M_w 1300), poly(glycidyl methacrylate) (PGMA, M_n = 150 539 kDa and polydispersity index 2.3, was a generous gift from Prof. Igor Luzinov and Dr. Bogdan Zydyrko, School of Materials Science and Engineering, Clemson University, Clemson, SC, USA), rhodamine B (RhB, Kodak, 95%), and 1,2-tetradecanediol (90%) were used as received.

Preparation of Multimodal Polymeric Nanoparticles. *Magnetite Synthesis.* Magnetite was prepared in accordance with the method described by Sun *et al.*[35] Briefly, iron(III) acetylacetonate (2 mM), 1,2-tetradecanediol (10 mM), oleic acid (6 mM), oleylamine (6 mM), and benzyl ether (20 mL) were mixed with a magnetic stirrer and gradually heated under a constant flow of N_2. The mixture was held at 100 °C for ~1 h before being ramped to 200 °C, held for 2 h, and finally heated to reflux (~300 °C) and held for 1 h under a blanket of N_2. The sample was allowed to cool to room temperature overnight under N_2 flow. The sample was collected and purified through a series of precipitations with ethanol; collection was via centrifugation and then resuspension in hexane, stored until use under argon.

PGMA Modification with Rhodamine B. PGMA (100 mg) and rhodamine B (20 mg) were dissolved in ethyl methyl ketone (30 mL) and heated to reflux under a N_2 atmosphere for 18 h. The PGMA-rhodamine-modified polymer was precipitated with diethyl ether and dried before use in nanoparticle production.

Multimodal Polymeric Nanoparticle Synthesis. Nanoparticles were prepared by an "oil in water" emulsion process. The organic phase contained magnetite nanoparticles (18 mg) and dissolved PGMA-rhodamine B (90 mg) in a 1:3 mixture of $CHCl_3$ and MEK (6 mL). The organic phase was added dropwise to a vortexing aqueous solution of Pluronic F108 (1.25% w/v, 30 mL), with the resulting microemulsion homogenized with a probe-type ultrasonicator for 1 min on low power. Organic solvents were allowed to evaporate under moderate stirring and N_2 flow overnight. Magnetite aggregates and unreacted polymer were removed via centrifugation (3000*g*, 45 min), with the supernatant being collected and incubated with PEI (50 wt % solution, 100 mg) at 70 °C for 20 h. The PEI-modified magnetic polymeric nanoparticles were collected on a magnetic separation column (LS, Miltenyi Biotec) and washed with milli-Q water to remove excess Pluronic and unattached dye before being collected, aliquoted, and stored. The equivalent dry mass of samples was determined by freeze-drying.

Nanoparticle Characterization. *Transmission Electron Microscopy (TEM).* Nanoparticle samples were prepared by deposition from water onto carbon-coated copper grids and imaged at 120 kV on a JEOL JEM-2100. Magentite samples were prepared by deposition from hexane onto carbon-coated copper grids and imaged at 120 kV on a JEOL JEM-2100.

Dynamic Light Scattering (DLS) and Zeta Potential Measurements. Nanoparticle samples were thoroughly washed (3× ~2 mL of Milli-Q water) while being held on a magnetic separation column (LS, Miltenyi Biotec) before being suspended in Milli-Q water for analysis.

Confocal Imaging. Confocal imaging was done on a Nikon Ti-E inverted motorized microscope with a Nikon A1Si spectral detector confocal system running NIS-C Elements software. Primary isolates of guinea pig cardiac myoctyes were incubated in MatTek glass bottom dishes and imaged live on the confocal, making use of the Tokai Hit Chamber microscope incubation system. Nanoparticles with NPs tethered with AID peptide and TAMRA-AID-TAT were incubated with myocytes at a final concentration of 1 μM peptide.

AID Peptide Attachment to PGMA Nanoparticles. AID peptide (160 nM) was incubated with 800 μg of nanoparticles (800 μL), 1 h at room temperature. The samples were then centrifuged 16000*g*, 30 min, the supernatant was collected, and aliquots of the supernatant were measured for absorbance at 280 nm using a NanoDrop UV–vis spectrophotometer. Peptide concentration in the supernatant was measured through comparison with the previously prepared standard curve (Figure S2, Supporting Information). The pellet containing nanoparticles and attached peptide was resuspended in a suitable volume to prepare a stock peptide conjugated to nanoparticles of 100 μM peptide. The conjugated stock samples were stored in glass vials for up to 1 month at 4 °C for ongoing use. The scramble peptide attached to nanoparticles was prepared following the same procedure.

Synthesis of AID Peptide. A peptide against the alpha-interacting domain in the I–II linker of the α_{1C} subunit was synthesized using the amino acid sequence QQLEEDLKGYLDWITQAE as previously described[36] (Auspep Pty Ltd., Parkville, Australia). A scrambled control was also synthesized (QKILGEWDLAQYTDQELE). A HIV-TAT protein sequence (RKKRRQRRR) was added to the active and scrambled peptide to produce AID-TAT and AID(S)-TAT, respectively.

Isolation of Guinea Pig Ventricular Myocytes. Cardiac myocytes were isolated from adult tricolor guinea pigs (*Cavea porcellis*) weighing between 200 and 250 g. Animals were anesthetized with an intraperitoneal injection of pentobarbitone sodium (240 mg/kg) prior to excision of the heart as approved by The Animal Ethics Committee of The University of Western Australia in accordance with the Australian Code of Practice for the Care and Use of Animals for Scientific Purposes (NH&MRC, seventh edition, 2004). Cells were isolated and cultured as described previously.[37,38]

Uptake Studies with Cardiac Myocytes. Uptake of AID-TAT and AID-tethered nanoparticles was monitored in freshly isolated myocytes by assessing alterations in TAMRA and rhodamine B fluorescence (ex 535 nm, em 580 nm) prior to and following addition of TAMRA-labeled AID-TAT and rhodamine B-labeled AID–nanoparticles, respectively, at 37 °C using a Hamamatsu Orca ER digital camera attached to an inverted Nikon TE2000-U microscope. Fluorescent images were taken at 5 min intervals with 200 ms exposure. Metamorph 6.3 was used to quantify the signal by manually tracing myocytes. An equivalent region not containing cells was used as background and was subtracted. Fluorescent values for each time point were plotted relative to an associated basal (pre) fluorescent value of 1.0.

Intracellular Ca^{2+} Levels: Fura-2 Assessment. Intracellular calcium was monitored in freshly isolated cardiac myocytes using the fluorescent indicator Fura-2 AM (Fura-2, 1 μM, ex 340/380 nm, em 510 nm, Molecular Probes) at 37 °C as previously described.[1] Fluorescence at 340/380 nm excitation and 510 nm emission were measured at 1 min intervals with an exposure of 50 ms on a Hamamatsu Orca ER digital camera attached to an inverted Nikon TE2000-U microscope. Ratiometric 340/380 nm signals of individual myocytes were quantified using Metamorph 6.3 to measure signal intensity of manually traced cell regions. An equivalent region not containing cells was used for background and was subtracted. Fluorescent ratios recorded over 3 min were averaged 7 min following addition of BayK(–) and reported as a percentage from the baseline pretreatment average.

Ischemia–Reperfusion Model. Hearts from adult tricolor guinea pigs were excised and perfused on a Langendorff apparatus with calcium-containing Krebs-Henseleit buffer (KHB) containing (in mM) 110 potassium glutamate, 25 KCl, 10 KH_2PO_4, 2 $MgSO_4$, 20 taurine, 5 creatine base, 5 HEPES, 20 glucose, 1.5 $CaCl_2$, 0.5 EGTA, pH 7.4 at 37 °C. Hearts were perfused for 30 min at a rate of 7 mL/min, followed by 30 min no-flow ischemia, then 30 min reperfusion as previously described.[39] Perfusates were collected 25 min preischemia and 10 min following reperfusion. AID-TAT peptide, AID(S)-TAT peptide, AID-tethered nanoparticles, or AID(S)-tethered nanoparticles were added to calcium-containing KHB solution just prior to reperfusion.

CK and LDH Assays. Creatine kinase and lactate dehydrogenase activity was determined from perfusate from ischemia–reperfused hearts as previously described.[40] CK activity was determined using a Randox CK NAC-activated diagnostic kit (Randox Laboratories). The rate of increase in absorbance was measured at 340 nm (PowerWave XS, BioTek) over 15 min at 30 °C. CK activity was calculated using the following equation:

$$\text{CKactivity (U/L)} = \frac{4127 \times (\Delta\text{Abs 340nm})}{\text{min}}$$

To determine LDH activity, 150 μL of perfusate sample was mixed with 50 μL of LDH assay buffer (50 mM imidazole, 375 μM NADH, 4 mM pyruvate, 0.05% BSA, pH 7.0), and the rate of decrease in absorbance was measured at 340 nm (PowerWave XS, BioTek) over 15 min at 25 °C. LDH activity was calculated using the following equation:

$$\text{LDH activity (U/mL)} = \frac{\left(\frac{\Delta\text{Abs 340 nm}}{\text{min TEST}} - \frac{\Delta\text{Abs 340 nm}}{\text{min BLANK}}\right) \times 3 \times (\text{dilution factor})}{(6.22)(0.1)}$$

Heart Biodistribution Studies. Guinea pig hearts were used for MRI analysis of NP distribution. Hearts of C57BL/10ScSnArc mice were used to assess distribution of TAT-AID-TAMRA fluorescence. After perfusion of AID-NPs or TAT-AID-TAMRA, hearts were stored in paraformaldehyde for fixation before MRI measurement. Following MRI, hearts where sectioned and mounted for fluorescence microscopy analysis on an Olympus IX71 inverted fluorescent microscope with an Olympus DP70 camera. Images were collected across heart sections at 4× magnification with a standard TRITC fluorescence filter and later stitched together making use of the MosaicJ FiJi Plugin.

MRI. Twelve hours prior to scanning, the four hearts were transferred to labeled 25 mL glass vials and immersed in standard saline solution (0.9% NaCl). For the MRI measurements, the four vials were secured to the base of a 1 L plastic container, and the container was filled with deionized water to surround the samples, reducing magnetic susceptibility differences.

All MRI measurements were made on a Phillips 3 T Achieva scanner (Royal Philips Electronics, Amsterdam, The Netherlands) at Sir Charles Gairdner Hospital, Western Australia. A 32-channel phased-array cardiac coil was centered over the sample container. Data acquisition comprised a multiecho spin echo sequence (TEs 20, 40, 60, 80, 100 ms, TR 4348 ms, 2 excitations). The slice thickness was 1 mm, and the reconstruction matrix was 448 × 448 with a field of view 130 × 130 mm. The transverse relaxation rate, R_2, was derived from pixelwise monoexponential fits to the signal intensity image data using ImageJ 1.45s (NIH, USA). In previous work,[30] R_2 was linearly related to the iron concentration of these PGMA nanoparticles; hence higher R_2 values are indicative of greater accumulation of nanoparticles in the heart tissue.

Statistical Analysis. Results are reported as mean ± SE. Statistical comparisons of responses between unpaired data were made using Student's *t* test or between groups of cells using one-way ANOVA and Tukey's posthoc test (GraphPad Prism version 5.04)

Conflict of Interest: The authors declare no competing financial interest.

Supporting Information Available: Reference peptide standard curve, confocal image of 1 μM AID tethered to nanoparticles with a cardiac myocyte, two confocal video Z-stack reconstructions of 1 μM AID tethered to nanoparticles with myocytes, and an assessment of intracellular superoxide levels after AID-NP treatment. This material is available free of charge *via* the Internet at http://pubs.acs.org.

Acknowledgment. The authors would like to acknowledge Prof. Igor Luzinov and Dr. Bogdan Zydyrko from the School of Materials Science and Engineering, Clemson University, Clemson, SC, USA, for the synthesis of the polyglycidyl methacrylate used to synthesis the polymeric nanoparticles. The authors would also like to thank A/Prof Paul Rigby, Dr. Tamara Abel, and Francis Yap for their technical help and expertise with the sectioning and confocal imaging in addition to the staff in the MRI Radiology Department at Sir Charles Gardiner Hospital, Perth, Australia, for radiological support. The authors acknowledge the Australian Microscopy & Microanalysis Research Facility at the Centre for Microscopy, Characterisation & Analysis, The University of Western Australia, funded by the University, State, and Commonwealth Governments. This work was funded by the Australian Research Council (ARC) and the National Health & Medical Research Council (NHMRC) of Australia. H.M.V. is a National Heart Foundation Research Fellow, and L.C.H. is an ARC Future Fellow and Honorary NHMRC Senior Research Fellow.

REFERENCES AND NOTES

1. Viola, H. M.; Arthur, P. G.; Hool, L. C. Transient Exposure to Hydrogen Peroxide Causes an Increase in Mitochondria-Derived Superoxide As a Result of Sustained Alteration in L-Type Ca^{2+} Channel Function in the Absence of Apoptosis in Ventricular Myocytes. *Circ. Res.* **2007**, *100*, 1036–1044.
2. Seenarain, V.; Viola, H. M.; Ravenscroft, G.; Casey, T. M.; Lipscombe, R. J.; Ingley, E.; Laing, N. G.; Bringans, S. D.; Hool, L. C. Evidence of Altered Guinea Pig Ventricular Cardiomyocyte Protein Expression and Growth in Response to a 5 min *in Vitro* Exposure to H_2O_2. *J. Proteome Res.* **2010**, *9*, 1985–1994.
3. Brookes, P. S.; Yoon, Y. S.; Robotham, J. L.; Anders, M. W.; Sheu, S. S. Calcium, ATP, and ROS: A Mitochondrial Love-Hate Triangle. *Am. J. Physiol.: Cell Physiol.* **2004**, *287*, 817–833.
4. Frey, N.; Olson, E. N. Cardiac Hypertrophy: The Good, the Bad and the Ugly. *Annu. Rev. Physiol.* **2003**, *65*, 45–79.
5. Pizzetti, G.; Mailhac, A.; Li Volsi, L.; Di Marco, F.; Lu, C.; Margonato, A.; Chierchia, S. L. Beneficial Effects of Diltiazem during Myocardial Reperfusion: A Randomized Trial in Acute Myocardial Infarction. *Ital. Heart J.* **2001**, *2*, 757–765.
6. Bestehorn, H. P.; Neumann, F. J.; Buttner, H. J.; Betz, P.; Sturzenhofecker, P.; von Hodenberg, E.; Verdun, A.; Levai, L.; Monassier, J. P.; Roskamm, H. Evaluation of the Effect of Oral Verapamil on Clinical Outcome and Angiographic Restenosis after Percutaneous Coronary Intervention: The Randomized, Double-Blind, Placebo-Controlled, Multicenter Verapamil Slow-Release for Prevention of Cardiovascular Events after Angioplasty (VESPA) Trial. *J. Am. Coll. Cardiol.* **2004**, *43*, 2160–2165.
7. Wang, Q. D.; Pernow, J.; Sjoquist, P. O.; Ryden, L. Pharmacological Possibilities for Protection Against Myocardial Reperfusion Injury. *Cardiovasc. Res.* **2002**, *55*, 25–37.
8. Romero, M.; Sanchez, I.; Pujol, M. D. New Advances in the Field of Calcium Channel Antagonists: Cardiovascular Effects and Structure-Activity Relationships. *Curr. Med. Chem.: Cardiovasc. Hematol. Agents* **2003**, *1*, 113–141.
9. Chernyak, B. V. Redox Regulation of the Mitochondrial Permeability Transition Pore. *Biosci. Rep.* **1997**, *17*, 293–302.
10. Berridge, M. J. Calcium Microdomains: Organization and Function. *Cell Calcium* **2006**, *40*, 405–412.
11. McCormack, J. G.; Halestrap, A. P.; Denton, R. M. Role of Calcium Ions in Regulation of Mammalian Intramitochondrial Metabolism. *Physiol. Rev.* **1990**, *70*, 391–425.

12. Bandyopadhyay, D.; Chattopadhyay, A.; Ghosh, G.; Datta, A. Oxidative Stress-Induced Ischemic Heart Disease: Protection by Antioxidants. *Curr. Med. Chem.* **2004**, *11*, 369–387.
13. Dhalla, N. S.; Elmoselhi, A. B.; Hata, T.; Makino, N. Status of Myocardial Antioxidants in Ischemia-Reperfusion Injury. *Cardiovasc. Res.* **2000**, *47*, 446–456.
14. Kilgore, K. S.; Friedrichs, G. S.; Johnson, C. R.; Schasteen, C. S.; Riley, D. P.; Weiss, R. H.; Ryan, U.; Lucchesi, B. R. Protective Effects of the Sod-Mimetic Sc-52608 against Ischemia/Reperfusion Damage in the Rabbit Isolated Heart. *J. Mol. Cell. Cardiol.* **1994**, *26*, 995–1006.
15. Downey, J. M.; Omar, B.; Ooiwa, H.; Mccord, J. Superoxide-Dismutase Therapy for Myocardial-Ischemia. *Free Radical Res. Commun.* **1991**, *12−3*, 703–720.
16. Ooiwa, H.; Stanley, A.; Felaneousbylund, A. C.; Wilborn, W.; Downey, J. M. Superoxide-Dismutase Conjugated to Polyethylene-Glycol Fails to Limit Myocardial Infarct Size after 30 min Ischemia Followed by 72 h of Reperfusion in the Rabbit. *J. Mol. Cell. Cardiol.* **1991**, *23*, 119–125.
17. Vanhaecke, J.; Vandewerf, F.; Ronaszeki, A.; Flameng, W.; Lesaffre, E.; Degeest, H. Effect of Superoxide-Dismutase on Infarct Size and Postischemic Recovery of Myocardial-Contractility and Metabolism in Dogs. *J. Am. Coll. Cardiol.* **1991**, *18*, 224–230.
18. Pragnell, M.; Dewaard, M.; Mori, Y.; Tanabe, T.; Snutch, T. P.; Campbell, K. P. Calcium-Channel Beta-Subunit Binds to a Conserved Motif in the I-II Cytoplasmic Linker of the Alpha 1-Subunit. *Nature* **1994**, *368*, 67–70.
19. Striessnig, J. Pharmacology, Structure and Function of Cardiac L-Type Ca^{2+} Channels. *Cell. Physiol. Biochem.* **1999**, *9*, 242–269.
20. Hohaus, A.; Person, V.; Behlke, J.; Schaper, J.; Morano, I.; Haase, H. The Carboxyl-Terminal Region of Ahnak Provides a Link between Cardiac L-Type Ca^{2+} Channels and the Actin-Based Cytoskeleton. *FASEB J.* **2002**, 16.
21. Brooks, H.; Lebleu, B.; Vives, E. TAT Peptide-Mediated Cellular Delivery: Back to Basics. *Adv. Drug Delivery Rev.* **2005**, *57*, 559–577.
22. Rapoport, M.; Lorberboum-Galski, H. TAT-Based Drug Delivery System - New Directions in Protein Delivery for New Hopes? *Expert Opin. Drug Delivery* **2009**, *6*, 453–463.
23. Herce, H.; Garcia, A. Molecular Dynamics Simulations Suggest a Mechanism for Translocation of the Hiv-1 TAT Peptide across Lipid Membranes. *Proc. Natl. Acad. Sci. U.S. A.* **2007**, *104*, 20805–20810.
24. Lundin, P.; Johansson, H.; Guterstam, P.; Holm, T.; Hansen, M.; Langel, U.; Andaloussi, S. Distinct Uptake Routes of Cell-Penetrating Peptide Conjugates. *Bioconjugate Chem.* **2008**, *19*, 2535–2542.
25. Fawell, S.; Seery, J.; Daikh, Y.; Moore, C.; Chen, L. L.; Pepinsky, B.; Barsoum, J. TAT-Mediated Delivery of Heterologous Proteins into Cells. *Proc. Natl. Acad. Sci. U.S.A.* **1994**, *91*, 664–668.
26. Krpetic, Z.; Saleemi, S.; Prior, I. A.; See, V.; Qureshi, R.; Brust, M. Negotiation of Intracellular Membrane Barriers by TAT-Modified Gold Nanoparticles. *ACS Nano* **2011**, *5*, 5195–5201.
27. de la Fuente, J.; Berry, C. Tat Peptide as an Efficient Molecule to Translocate Gold Nanoparticles into the Cell Nucleus. *Bioconjugate Chem.* **2005**, *16*, 1176–1180.
28. Jones, S. W.; Christison, R.; Bundell, K.; Voyce, C. J.; Brockbank, S. M.; Newham, P.; Lindsay, M. A. Characterisation of Cell-Penetrating Peptide-Mediated Peptide Delivery. *Br. J. Pharmacol.* **2005**, *145*, 1093–1102.
29. Gump, J. M.; Dowdy, S. F. TAT Transduction: The Molecular Mechanism and Therapeutic Prospects. *Trends Mol. Med.* **2007**, *13*, 443–448.
30. Evans, C. W.; Fitzgerald, M.; Clemons, T. D.; House, M. J.; Padman, B. S.; Shaw, J. A.; Saunders, M.; Harvey, A. R.; Zdyrko, B.; Luzinov, I.; *et al.* Multimodal Analysis of PEI-Mediated Endocytosis of Nanoparticles in Neural Cells. *ACS Nano* **2011**, *5*, 8640–8648.
31. Harrison, J.; Bartlett, C. A.; Cowin, G.; Nicholls, P. K.; Evans, C. W.; Clemons, T. D.; Zdyrko, B.; Luzinov, I. A.; Harvey, A. R.; Iyer, K. S.; *et al.* *In Vivo* Imaging and Biodistribution of Multimodal Polymeric Nanoparticles Delivered to the Optic Nerve. *Small* **2012**, *8*, 1579–1589.
32. Bers, D. M. Cardiac Excitation-Contraction Coupling. *Nature* **2002**, *415*, 198–205.
33. Hool, L. C.; Corry, B. Redox Control of Calcium Channels: From Mechanisms to Therapeutic Opportunities. *Antioxid. Redox Signaling* **2007**, *9*, 409–435.
34. Viola, H. M.; Arthur, P. G.; Hool, L. C. Evidence for Regulation of Mitochondrial Function by the L-Type Ca^{2+} Channel in Ventricular Myocytes. *J. Mol. Cell. Cardiol.* **2009**, *46*, 1016–1026.
35. Sun, S.; Zeng, H.; Robinson, D.; Raoux, S.; Rice, P.; Wang, S.; Li, G. Monodisperse MFe_2O_4 (M = Fe, Co, Mn) Nanoparticles. *J. Am. Chem. Soc.* **2004**, *126*, 273–279.
36. Hohaus, A.; Poteser, M.; Romanin, C.; Klugbauer, N.; Hofmann, F.; Morano, I.; Haase, H.; Groschner, K. Modulation of the Smooth-Muscle L-Type Ca^{2+} Channel Alpha 1 Subunit (Alpha 1C-B) by the Beta 2a Subunit: A Peptide Which Inhibits Binding of Beta to the I-II Linker of Alpha 1 Induces Functional Uncoupling. *Biochem. J.* **2000**, *348*, 657–665.
37. Hool, L. C. Hypoxia Increases the Sensitivity of the L-Type Ca^{2+} Current to Beta-Adrenergic Receptor Stimulation via a C2 Region-Containing Protein Kinase C Isoform. *Circ. Res.* **2000**, *87*, 1164–1171.
38. Hool, L. C.; Di Maria, C. A.; Viola, H. M.; Arthur, P. G. Role of Nad(P)H Oxidase in the Regulation of Cardiac L-Type Ca^{2+} Channel Function during Acute Hypoxia. *Cardiovasc. Res.* **2005**, *67*, 624–635.
39. Hotta, Y.; Fujita, M.; Nakagawa, J.; Ando, H.; Takeya, K.; Ishikawa, N.; Sakakibara, J. Contribution of Cytosolic Ionic and Energetic Milieu Change to Ischemia- and Reperfusion-Induced Injury in Guinea Pig Heart: Fluorometry and Nuclear Magnetic Resonance Studies. *J. Cardiovasc. Pharmacol.* **1998**, *31*, 146–156.
40. Tang, H.; Viola, H. M.; Filipovska, A.; Hool, L. C. Ca(V)1.2 Calcium Channel Is Glutathionylated during Oxidative Stress in Guinea Pig and Ischemic Human Heart. *Free Radical Biol. Med.* **2011**, *51*, 1501–1511.